Giant Magnetoelastic-Coupling Driven Spin-Lattice Liquid State in Molybdate Pyrochlores

Andrew Smerald[1,*] and George Jackeli[1,2,†]
[1]Max Planck Institut für Festkörperforschung, Heisenbergstraße 1, D-70569 Stuttgart, Germany
[2]Insitute for Functional Matter and Quantum Technologies, University of Stuttgart, Pfaffenwaldring 57, D-70569 Stuttgart, Germany

(Received 20 December 2018; revised manuscript received 29 March 2019; published 7 June 2019)

We propose the idea of a spin-lattice liquid, in which spin and lattice degrees of freedom are strongly coupled and remain disordered and fluctuating down to low temperatures. We show that such a state arises naturally from a microscopic analysis of a class of molybdate pyrochlore compounds, and is driven by a giant magnetoelastic effect. Finally, we argue that this could explain some of the experimental features of $Y_2Mo_2O_7$.

DOI: 10.1103/PhysRevLett.122.227202

Introduction.—Frustration is at the heart of the search for unusual states of matter, and can promote spin-liquid behavior, in which the spins remain disordered and fluctuating down to low temperature [1–3]. However, the interaction of spins with lattice degrees of freedom (d.o.f.) is typically expected to result in long-range order via an "order-by-disorder"-type mechanism [4,5]. For example, magnetoelastic coupling can drive a structural distortion that selects a small subset of the otherwise extensively degenerate spin configurations [6–13]. Nevertheless, there is the intriguing possibility that spin and lattice d.o.f. can become tightly coupled, but, rather than ordering, remain fluctuating at low temperature, and we dub the resultant state a spin-lattice liquid.

In order to identify candidate materials for such a spin-lattice liquid state, there are a number of characteristic features that are required. These include strong magnetoelastic coupling, an absence of spin ordering at temperatures well below the interaction energy, and evidence for incoherently disordered lattice d.o.f. at low temperature. All of these characteristics have been experimentally observed in the pyrochlore molybdates, $R_2Mo_2O_7$ ($R = \mathrm{Y, Tb, Dy, Ho, Er, Tm, Yb, Lu}$ [14,15]), of which $Y_2Mo_2O_7$ is the best studied example [16–28]. However, many aspects of their low-temperature behavior remain mysterious, despite more than three decades of study.

In this Letter we analyze the Mo pyrochlores and show that at intermediate temperatures they may support a state in which spin and lattice d.o.f. become strongly coupled and explore an extensive manifold of degenerate configurations. This state, which we refer to as a spin-lattice liquid, both serves as a first example of a class of states, as well as providing an explanation for the unusual behavior of the $R_2Mo_2O_7$ materials. We use microscopic analysis to show that spin-orbital and lattice d.o.f. would individually be expected to show behavior similar to the classical spin-liquid "spin ice" [29]. However, due to strong magnetoelastic coupling, a spin-lattice liquid phase emerges at low temperature. Since the magnetoelastic coupling plays a decisive and nonperturbative role in selecting the low-energy configurations, we refer to it as a "giant" magnetoelastic effect.

The $R_2Mo_2O_7$ materials crystallize into the well-known $Fd\bar{3}m$ space group, where Mo^{4+} ions form a pyrochlore lattice of corner-sharing tetrahedra and are surrounded by oxygen octahedra [17] [see Figs. 1(a) and 1(b)]. At low temperature ($T_f \approx 20$ K) a spin-glass transition is observed [16,20], whose origin remains an open question [15]. However, this occurs well below the Curie-Weiss temperature ($\theta_{\mathrm{cw}} = -200$ K for $Y_2Mo_2O_7$ [30]), which approximately measures the strength of magnetic interactions. As such there is a wide temperature range, $T_f < T < \theta_{\mathrm{cw}}$ in which spin correlations are expected to be significant, but no spin ordering is observed.

At the same time, extensive studies of the crystal structure have shown that there are significant low-temperature local distortions away from the average $Fd\bar{3}m$ structure that survive up to temperatures in excess of θ_{cw}, but no structural phase transition [22–26,28]. Recent pair-distribution function analysis has shown that for each tetrahedron two Mo^{4+} ions move towards and two away from the tetrahedral center, forming a highly degenerate "2-in-2-out" distortion pattern [28] [see Fig. 1(c)]. There is a concomitant distortion of the O octahedra, such that both the Mo—O bond length and the local crystal field remains almost invariant. However, the nearest-neighbor Mo—Mo distances and the Mo—O—Mo bond angles change significantly.

Magnetoelastic coupling provides a link between the spin and lattice d.o.f., and there is evidence from NMR and μsr measurements that it is significant in $Y_2Mo_2O_7$ [23,24,26]. As a consequence, the experimental prerequisites appear to be in place to think the $R_2Mo_2O_7$ materials

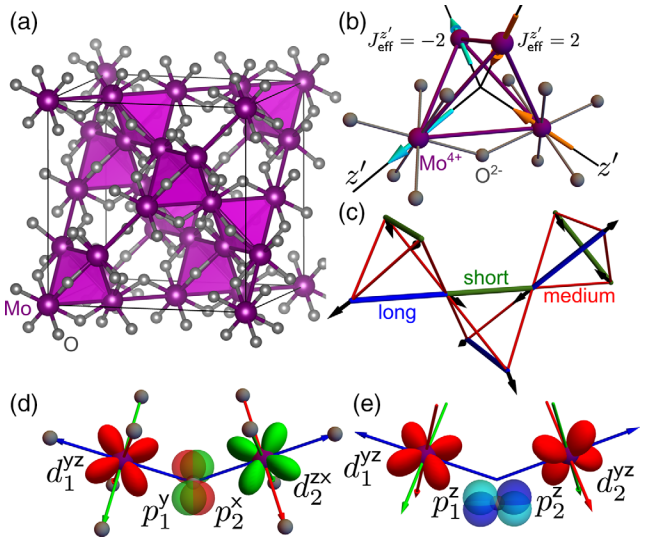

FIG. 1. $R_2Mo_2O_7$ pyrochlores. (a) Average $Fd\bar{3}m$ structure of $R_2Mo_2O_7$, showing the Mo pyrochlore lattice (purple) and surrounding O octahedra (gray) within a unit cell (black cuboid). (b) $J^{z'}_{\rm eff}=\pm 2$ states are represented by arrows pointing in or out of the Mo tetrahedron along the z' local axes. (c) 2-in-2-out lattice displacements (black arrows) create one long (blue), four medium (red), and one short (green) Mo—Mo bond on each tetrahedron. (d) π-type dpd hopping path, shown for idealized regular oxygen octahedra. The path shown is $d^{yz}_1-(p^y_1:p^x_2)-d^{yz}_2$, where Mo sites are labeled 1 and 2 and have associated local coordinates (x, red; y, green; z, blue). (e) σ-type hopping path allowed by trigonal distortion of the oxygen octahedra and exemplified by $d^{yz}_1-(p^z_1:p^z_2)-d^{yz}_2$.

may realize a spin-lattice liquid state. In order to explore whether this is the case, we use microscopic arguments to understand the interplay between spin, orbital, and lattice, and derive a simple effective model in an attempt to capture the essence of their low-temperature behavior.

Local electronic states.—The starting point is to consider the local physics of the Mo^{4+} ions. Mo^{4+} has two electrons in the $4d$ shell, and these are localized by an on-site Coulomb repulsion U that is large compared to the bandwidth [15]. The local cubic crystal field due to the surrounding O^{2-} octahedron [see Figs. 1(a) and 1(b)] splits the $4d$ energy levels into a low-energy t_{2g} manifold of xy, yz, and zx orbitals that point between the O ions, and a high-energy e_g manifold of orbitals pointing towards O ions [31]. The t_{2g} manifold is split by Hund's coupling ($J_H\approx 0.5$ eV [32]), which favors parallel spins, and therefore selects a ninefold degenerate set of low-energy states, labeled by spin $S=1$ and effective orbital angular momentum $L_{\rm eff}=1$ [33]. This is further split by a noncubic component of the crystal field with trigonal symmetry that results from a compression of O octahedra along the local z' axes pointing into or out of Mo tetrahedra [see Fig. 1(b)] and spin-orbit coupling. The characteristic energy scales are, respectively, $\Delta_{\rm trig}\approx 160$ meV and $\lambda_{\rm SO}\approx 40$ meV [32]. The result is a low-energy doublet, labeled as $J^{z'}_{\rm eff}=\pm 2$, where $\mathbf{J}_{\rm eff}=\mathbf{S}+\mathbf{L}_{\rm eff}$, that is separated from the first excited state by an energy gap $\Delta E=\lambda_{\rm SO}[1-\lambda_{\rm SO}/\Delta_{\rm trig}+\ldots]\approx 30$ meV$\approx$300 K ($k_B=1$) [34].

Exchange interaction.—An effective low-energy model can be derived by considering superexchange interactions between neighboring $J^{z'}_{\rm eff}=\pm 2$ doublets. This is different from previous approaches that assume an isotropic $S=1$ spin on every site [40–42]. The geometry is simplest in the case of idealized undistorted oxygen octahedra, where local cubic axes can be aligned with the O octahedra [Fig. 1(d)]. Superexchange occurs via a single intermediate oxygen with Mo—O—Mo bond angle $\alpha=2\arctan 2\sqrt{2}\approx 141°$. Within the local cubic axes the dominant hopping channel is off diagonal, bond dependent, and follows paths of the type $d^{yz}_1-(p^y_1:p^x_2)-d^{zx}_2$, where p^y_1 and p^x_2 denote orbitals on the same oxygen ion but in the local axes of the two different Mo ions [1 and 2 in Fig. 1(d)]. It can be seen that the d—p bonds involve a lateral overlap of orbitals, and this is known as π bonding [43].

We work in the Mott insulator picture, where, for two electrons in the t_{2g} manifold, the derivation of a spin-orbital Hamiltonian from a multiorbital Hubbard model is a standard procedure [34,44–46]. Projection into the $J^{z'}_{\rm eff}=\pm 2$ doublet results in the effective Hamiltonian taking the form of a classical Ising model, $\mathcal{H}_{\rm is}=J_{\rm is}\sum_{\langle ij\rangle}\sigma_i\sigma_j$ [34], where $\sigma=\pm 1$ labels the doublet states in terms of an Ising "spin" pointing into or out of tetrahedra [see Fig. 1(b)]. $J_{\rm is}>0$ favors antiferromagnetic alignment in the local trigonal axes, and low-energy states consist of the extensively degenerate spin-ice configurations with a 2-in-2-out arrangement. $J_{\rm is}<0$ favors ferromagnetic alignment in the local trigonal axes, and therefore unfrustrated all in or all out arrangements on tetrahedra. In the case of undistorted cubic octahedra we find $J_{\rm is}<0$ for any value of J_H/U.

In reality the oxygen octahedra are trigonally distorted, and in $Y_2Mo_2O_7$ the Mo—O—Mo bond angle in the average $Fd\bar{3}m$ structure is $\alpha=\alpha_{\rm av}=127°$ [17,25,28]. The displacement of the O relative to the undistorted case opens up a σ-type hopping channel, where orbitals directly overlap one another [43], and this is exemplified by the path $d^{yz}_1-(p^z_1:p^z_2)-d^{yz}_2$ shown in Fig. 1(e). The σ channel becomes comparable to the original π-bonding channel for a relatively small trigonal distortion, and as a result $J_{\rm is}>0$ for $\alpha=127°$, favoring a 2-in-2-out set of low-energy configurations [34].

Due to the competition between the π and σ channels, the value of $J_{\rm is}$ is extremely sensitive to the bond angle, as shown in Fig. 2(a). Serendipitously, the bond angle at which the exchange interaction cancels is close to $\alpha=\alpha_{\rm av}=127°$, both in our simple analytical calculations and also in more involved band structure calculations [32]. Deviations of the Mo—O—Mo bond angle from its average value thus lead to very large relative changes in $J_{\rm is}$.

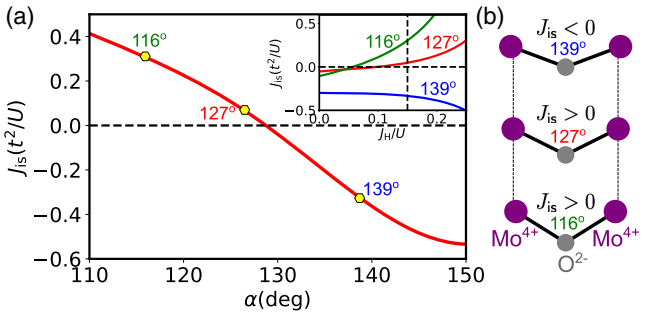

FIG. 2. Dependence of the Ising exchange interaction J_{is} on the Mo—O—Mo bond angle α. (a) J_{is} is plotted for $J_H/U = 0.15$ and measured in units of t^2/U, where $t = V_{pd\pi}^2/\Delta_{dp}$ is the hopping integral along a Mo—O—Mo π-type bond [34,47]. For σ bonds we use $V_{pd\sigma} = -2.2V_{pd\pi}$ [43]. The experimentally determined bond angles for $Y_2Mo_2O_7$ are marked [28] and J_{is} passes through zero close to the average bond angle, $\alpha_{av} \approx 127°$. (Inset) Dependence of J_{is} on J_H/U for $\alpha = 116°$ (green), $\alpha = 127°$ (red), and $\alpha = 139°$ (blue). (b) Experimentally determined bond angles for $Y_2Mo_2O_7$ [28].

In addition to the trigonal distortion, it is also necessary to take into account the 2-in-2-out distortions of the Mo ions, and concomitant movement of the O octahedra, which leaves the Mo—O bond length and local crystal field almost invariant, but significantly changes the Mo—Mo distances and the Mo—O—Mo bond angles [28]. The result is three classes of Mo—Mo bonds with significantly different exchange couplings [see Fig. 1(c)]. Combining the pair-distribution-function analysis with the calculations yields on each tetrahedron one short bond with $\alpha < \alpha_{av}$ and $J_{is} > 0$, four medium bonds with $\alpha \approx \alpha_{av}$ and $J_{is} > 0$ and one long bond with $\alpha > \alpha_{av}$ and $J_{is} < 0$. The magnitude of J_{is} is significantly larger on the short and long bonds than the medium bonds, resulting in a very strong magnetoelastic coupling effect.

Spin-lattice model.—Next, we consider the minimal effective model that captures the essence of the microscopic analysis. Mo lattice sites are allowed to displace in a 2-in-2-out pattern [Fig. 1(c)], corresponding to the triplet normal mode of a tetrahedron [6,8,11]. The resultant bond angles are $\alpha = \alpha_{av} + \delta\alpha$ on the long bond, $\alpha = \alpha_{av}$ on the medium bonds, and $\alpha = \alpha_{av} - \delta\alpha$ on the short bond, with $\delta\alpha \geq 0$ [see Fig. 2(b)]. For simplicity, $\delta\alpha$ is allowed to vary globally but not locally. Spins are constrained to point into or out of tetrahedra and described by $\sigma = \pm 1$. The resultant spin-lattice Hamiltonian is

$$\mathcal{H}_{sl} = \sum_{\langle ij \rangle} \{[J_{is}(\alpha_{av}) - g\delta\alpha_{ij}]\sigma_i\sigma_j + K\delta\alpha_{ij}^2\}, \qquad (1)$$

where $J_{is}(\alpha_{av})$ is the superexchange interaction for undistorted bonds, $g = \partial J_{is}/\partial\alpha|_{\alpha=\alpha_{av}}$ describes at first order the angular dependence of the interaction, $\delta\alpha_{ij} \in \{-\delta\alpha, 0, \delta\alpha\}$, and K is the elastic energy cost of distorting the lattice.

The nature of the ground state can be understood starting from a single tetrahedron, and depends on the ratio $g^2/[4KJ_{is}(\alpha_{av})]$. For $g^2/(4K) < J_{is}(\alpha_{av})$ it is energetically favorable to have $\delta\alpha(T = 0) = \delta\alpha_{gs} = 0$ combined with a 2-in-2-out spin configuration on each tetrahedra, and as a result a spin ice forms at low T. For $g^2/(4K) > J_{is}(\alpha_{av})$ the lowest energy is reached with $\delta\alpha_{gs} = g/(2K)$, and writing $J_{is}(\alpha) = J_{is}(\alpha_{av}) \pm \delta J_{is}$, one finds $\delta J_{is} > 2J_{is}(\alpha_{av})$ on long and short bonds. For a given lattice distortion a tetrahedron has four degenerate low-energy 3-1 spin configurations, where 3 spins point in and 1 out or vice versa, as shown in the inset of Fig. 3 [48]. The combined manifold of spin and lattice configurations is extensive [34], and so a spin-lattice liquid may be realized at low T.

The full phase diagram can be explored using Monte Carlo simulation, and is shown in Fig. 3 [34]. We set $g/(2K) = 0.2$, since this corresponds to the experimental findings at low T [28]. As expected, for $g^2/(4K) < J_{is}(\alpha_{av})$ there is no lattice distortion at any temperature, and, below a specific heat peak at $T \approx 0.8J_{is}$, the system shows the characteristic behavior of spin ice.

For $g^2/(4K) > J_{is}(\alpha_{av})$ there are two transitions as the temperature is reduced, and this can be seen in simulations of the heat capacity shown in Fig. 4(a). At $T = T_1$ there is a first-order liquid-gas-like transition in which $\delta\alpha(T)$ jumps discontinuously from $\delta\alpha(T > T_1) \approx 0$ to $\delta\alpha(T = T_1^-) \approx J_{is}(\alpha_{av})/g$. Below this there are three classes of bonds, long and short bonds with coupling $J_{is}(\alpha_{av}) \pm g\delta\alpha(T)$ and medium bonds with coupling $J_{is}(\alpha_{av})$ (Fig. 3). For a fixed lattice configuration, the long and short bonds form nonintersecting loops that visit every lattice site and on which the sign of the coupling alternates. Strong spin

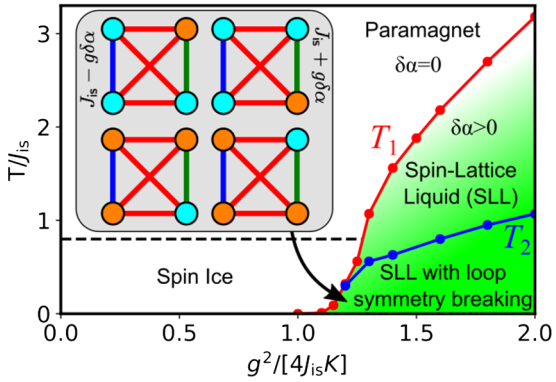

FIG. 3. Phase diagram of $\mathcal{H}_{sl}$ [Eq. (1)] from Monte Carlo simulation. For $g^2/(4K) < J_{is}$ there is no lattice distortion and a crossover (dashed line) to spin-ice behavior occurs at low T. For $g^2/(4K) > J_{is}$ an incoherent lattice distortion occurs ($\delta\alpha > 0$) and a spin-lattice liquid (SLL) forms below a first-order transition (red). At lower T a likely second-order transition (blue) picks out loops of length $l_{loop} = 4m + 4$, $m = 1, 2, \ldots$ [34]. (Inset) Four degenerate 3-1 ground states of a tetrahedron in the SLL state with a fixed lattice distortion (short bond in green and long bond in blue), and with spins pointing in (orange) and out (blue).

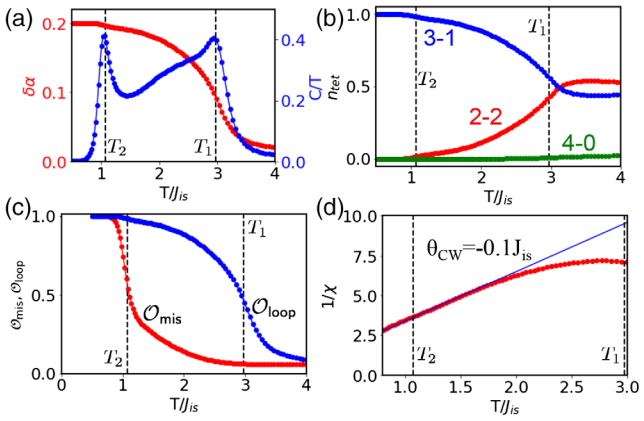

FIG. 4. Physical characteristics of $\mathcal{H}_{\rm sl}$ [Eq. (1)] from Monte Carlo simulation for $g^2/(4K) = 2J_{\rm is}$. Error bars are smaller than the point sizes. (a) Lattice distortion $\delta\alpha$ and heat capacity C/T showing two transitions. Results are shown for $L = 3$ (total number of spins $N = 16L^3$), for which equilibration is possible across the lower-T transition, and are consistent with simulations with larger L [34]. (b) Fraction of tetrahedra displaying 2-in-2-out (red), 3-1 (blue), or 4-0 (green) spin configurations. (c) Loop-based order parameters showing spin correlations on loops $\mathcal{O}_{\rm loop}$ and mismatch between loops of length $l_{\rm loop} = 4m + 2$ and $l_{\rm loop} = 4m + 4$, $\mathcal{O}_{\rm mis}$ [34]. (d) Inverse magnetic susceptibility. The fit to $1/\chi \propto T - \theta_{\rm cw}$ gives $\theta_{\rm cw} = -0.1J_{\rm is}$.

correlations form on these loops at the transition temperature, favoring alternating pairs of $\sigma = \pm 1$ [34]. The correlations increase on further decreasing T, and this is related to the increasing density of tetrahedra with a 3-1 spin configuration [see Fig. 4(b)]. The loops themselves are not static, but constantly rearrange themselves subject to the 2-in-2-out constraint on the lattice displacements [34].

At lower T there is a transition at $T = T_2$ that is likely second order, and in which the system excludes loops with length $l_{\rm loop} = 4m + 2$ ($m = 1, 2, \ldots$) in favor of those with length $l_{\rm loop} = 4m + 4$, which we call loop symmetry breaking [see Fig. 4(c)and [34]]. This occurs because loops with length $l_{\rm loop} = 4m + 2$ cannot simultaneously minimize the energy of every bond, unlike loops with length $l_{\rm loop} = 4m + 4$ [34]. Below $T = T_2$ essentially all tetrahedra adopt a 3-1 spin configuration [Fig. 4(b)] and the energy saturates, but the number of allowed configurations remains extensive.

The essence of the resultant spin-lattice liquid state is that it is built by nonperturbatively coupling two classical spin liquids, which in the present case are both spin ice. As with classical spin liquids, spin-lattice liquids can be described by a coarse-grained gauge theory, and, while this inherits some of the structure of the underlying spin-liquid gauge theories [53,54], the nonperturbative coupling provides additional constraints on the allowed configurations. A detailed exploration of such an effective field theory is left for future work.

Relation to experiment.—In order to determine an approximate value of the control parameter $g^2/[4KJ_{\rm is}(\alpha_{\rm av})]$ for $Y_2Mo_2O_7$, the calculated value of $g/J_{\rm is}(\alpha_{\rm av}) \sim 20$ can be combined with the experimentally determined $\delta\alpha_{\rm gs} = g/(2K) \approx 0.2$ [28], to give $g^2/[4KJ_{\rm is}(\alpha_{\rm av})] \sim 2$, placing the material on the right of the phase diagram in Fig. 3.

The predictions of the model are predominantly aimed at understanding the intermediate temperature regime of $Y_2Mo_2O_7$, above the spin-glass freezing temperature T_f, but below the energy of the first crystal-field excitation ΔE. This should be compared with the model in the region $T_2 < T < T_1$. Here, the discreteness of the Ising d.o.f., coupled with the discrete distortions of the Mo ions provide an explanation for the multiple peaks observed in NMR spectra of Y nuclei [23]. It is also consistent with the finding in μsr and NMR $1/T_2$ measurements that the lattice distortions are temperature dependent and respond strongly to magnetic field [24,26].

At lower temperatures the degeneracy of the model means that other subdominant effects are likely to play a role. To understand the experimentally observed spin-glass region ($T \leq T_f$) it is likely necessary to take into account some combination of disorder, further-neighbor interactions and additional exchange couplings arising from higher-energy crystal-field levels. In particular, small local changes in the Mo—O—Mo bond angle (i.e., in $\delta\alpha$) will result in additional disorder in the exchange couplings. One promising feature of the model is that its highly correlated low-temperature dynamics likely make it very susceptible to spin-glass freezing, particularly in the vicinity of T_2, where Monte Carlo simulations become difficult to equilibrate.

At high temperatures ($T \sim \Delta E \sim 300$ K) the excited crystal-field levels become thermally populated, and therefore the approximation of being in the low-energy doublet breaks down. Since ΔE is smaller than the temperature at which NMR linewidth extrapolations determine that the lattice distortion dies away (~430 K) [23], the first-order transition predicted by the model is likely smeared out due to the additional local d.o.f. and the opening of new hopping pathways.

A particular mystery in $Y_2Mo_2O_7$ is why susceptibility measurements show a negative (AFM) Curie-Weiss temperature of $\theta_{\rm cw} \approx -200$ K in the high temperature range 500–800 K [30], a different Curie-Weiss temperature of $\theta_{\rm cw} \approx -41$ K in the intermediate range 50–300 K [27] but ring features surrounding the Γ point in low-temperature neutron-scattering measurements that can only be explained by including FM coupling [27]. Our model provides a resolution by proposing a mechanism by which AFM and FM interactions can coexist. Simulations in the temperature range $T_2 < T < T_1$ show an emergent Curie-Weiss behavior with $\theta_{\rm cw} < 0$ [see Fig. 4(d)], despite the presence of strong correlations. Above $T \sim 300$ K the local electronic state is no longer confined to the ground state

doublet, and a change in the Curie-Weiss behavior is unsurprising.

In conclusion, we have proposed the idea of a spin-lattice liquid state, arising from strong coupling between two "spin" liquids, one associated with the spin-orbital and the other with the lattice d.o.f. Furthermore, we have shown that it may be realized in $Y_2Mo_2O_7$ and related compounds, driven by a giant magnetoelastic coupling effect. According to our theory, the strength of the magnetoelastic coupling is the main thing that distinguishes the molybdate pyrochlores from f-electron spin-ice compounds such as $Dy_2Ti_2O_7$ [29]. Finally, we end with the hope that other materials may be found, in which the dance of spin and lattice extends down to even lower temperature.

We thank Reinhard Kremer, Ludovic Jaubert, Joe Paddison, and Hidenori Takagi for useful comments on the manuscript. G. J. acknowledges support from the Alexander von Humboldt Foundation.

*andrew.smerald@gmail.com
†Also at Andronikashvili Institute of Physics, 0177 Tbilisi, Georgia.

[1] C. Lacroix, P. Mendels, and F. Mila, *Introduction to Frustrated Magnetism* (Springer, New York, 2011).
[2] L. Balents, Nature (London) **464**, 199 (2010).
[3] L. Savary and L. Balents, Rep. Prog. Phys. **80**, 016502 (2016).
[4] J. Villain, R. Bidaux, J.-P. Carton, and R. Conte, J. Phys. France **41**, 1263 (1980).
[5] E. F. Shender, Zh. Eksp. Teor. Fiz. **83**, 326 (1982) [Sov. Phys. JETP **56**, 178 (1982)].
[6] Y. Yamashita and K. Ueda, Phys. Rev. Lett. **85**, 4960 (2000).
[7] O. Tchernyshyov, R. Moessner, and S. L. Sondhi, Phys. Rev. Lett. **88**, 067203 (2002).
[8] O. Tchernyshyov, R. Moessner, and S. L. Sondhi, Phys. Rev. B **66**, 064403 (2002).
[9] K. Penc, N. Shannon, and H. Shiba, Phys. Rev. Lett. **93**, 197203 (2004).
[10] S. Di Matteo, G. Jackeli, C. Lacroix, and N. B. Perkins, Phys. Rev. Lett. **93**, 077208 (2004).
[11] S. Di Matteo, G. Jackeli, and N. B. Perkins, Phys. Rev. B **72**, 024431 (2005).
[12] D. L. Bergman, R. Shindou, G. A. Fiete, and L. Balents, Phys. Rev. B **74**, 134409 (2006).
[13] N. Shannon, K. Penc, and Y. Motome, Phys. Rev. B **81**, 184409 (2010).
[14] L. Clark, C. Ritter, A. Harrison, and J. Attfield, J. Solid State Chem. **203**, 199 (2013).
[15] H. Shinaoka, Y. Motome, T. Miyake, S. Ishibashi, and P. Werner, arXiv:1810.09596.
[16] J. Greedan, M. Sato, X. Yan, and F. Razavi, Solid State Commun. **59**, 895 (1986).
[17] J. Reimers, J. Greedan, and M. Sato, J. Solid State Chem. **72**, 390 (1988).
[18] N. P. Raju, E. Gmelin, and R. K. Kremer, Phys. Rev. B **46**, 5405 (1992).
[19] S. R. Dunsiger, R. F. Kiefl, K. H. Chow, B. D. Gaulin, M. J. P. Gingras, J. E. Greedan, A. Keren, K. Kojima, G. M. Luke, W. A. MacFarlane, N. P. Raju, J. E. Sonier, Y. J. Uemura, and W. D. Wu, J. Appl. Phys. **79**, 6636 (1996).
[20] M. J. P. Gingras, C. V. Stager, N. P. Raju, B. D. Gaulin, and J. E. Greedan, Phys. Rev. Lett. **78**, 947 (1997).
[21] J. S. Gardner, B. D. Gaulin, S.-H. Lee, C. Broholm, N. P. Raju, and J. E. Greedan, Phys. Rev. Lett. **83**, 211 (1999).
[22] C. H. Booth, J. S. Gardner, G. H. Kwei, R. H. Heffner, F. Bridges, and M. A. Subramanian, Phys. Rev. B **62**, R755 (2000).
[23] A. Keren and J. S. Gardner, Phys. Rev. Lett. **87**, 177201 (2001).
[24] E. Sagi, O. Ofer, A. Keren, and J. S. Gardner, Phys. Rev. Lett. **94**, 237202 (2005).
[25] J. E. Greedan, D. Gout, A. D. Lozano-Gorrin, S. Derahkshan, T. Proffen, H.-J. Kim, E. Božin, and S. J. L. Billinge, Phys. Rev. B **79**, 014427 (2009).
[26] O. Ofer, A. Keren, J. S. Gardner, Y. Ren, and W. A. MacFarlane, Phys. Rev. B **82**, 092403 (2010).
[27] H. J. Silverstein, K. Fritsch, F. Flicker, A. M. Hallas, J. S. Gardner, Y. Qiu, G. Ehlers, A. T. Savici, Z. Yamani, K. A. Ross, B. D. Gaulin, M. J. P. Gingras, J. A. M. Paddison, K. Foyevtsova, R. Valenti, F. Hawthorne, C. R. Wiebe, and H. D. Zhou, Phys. Rev. B **89**, 054433 (2014).
[28] P. M. M. Thygesen, J. A. M. Paddison, R. Zhang, K. A. Beyer, K. W. Chapman, H. Y. Playford, M. G. Tucker, D. A. Keen, M. A. Hayward, and A. L. Goodwin, Phys. Rev. Lett. **118**, 067201 (2017).
[29] S. T. Bramwell and M. J. P. Gingras, Science **294**, 1495 (2001).
[30] J. S. Gardner, G. Ehlers, S. T. Bramwell, and B. D. Gaulin, J. Phys. Condens. Matter **16**, S643 (2004).
[31] P. Fazekas, *Lecture Notes on Electron Correlation and Magnetism* (World Scientific, Singapore, 1999).
[32] H. Shinaoka, Y. Motome, T. Miyake, and S. Ishibashi, Phys. Rev. B **88**, 174422 (2013).
[33] A. Abragam and B. Bleaney, *Electron Paramagnetic Resonance of Transition Ions* (Oxford University Press, Oxford, 1970).
[34] See Supplemental Material at http://link.aps.org/supplemental/10.1103/PhysRevLett.122.227202 for more information concerning the local electronic state, the super-exchange Hamiltonian and Monte Carlo simulations of the spin-lattice model $\mathcal{H}_{sl}$, and including Refs. [35–39].
[35] D. Pesin and L. Balents, Nat. Phys. **6**, 376 (2010).
[36] C. Castellani, C. R. Natoli, and J. Ranninger, Phys. Rev. B **18**, 4945 (1978).
[37] L. D. C. Jaubert, Topological constraints and defects in spin ice, Ph.D. thesis, ENS Lyon, 2009.
[38] L. D. C. Jaubert, M. Haque, and R. Moessner, Phys. Rev. Lett. **107**, 177202 (2011).
[39] J. A. M. Paddison, Acta Crystallogr. Sect. A **75**, 14 (2019).
[40] T. E. Saunders and J. T. Chalker, Phys. Rev. Lett. **98**, 157201 (2007).
[41] A. Andreanov, J. T. Chalker, T. E. Saunders, and D. Sherrington, Phys. Rev. B **81**, 014406 (2010).
[42] H. Shinaoka, Y. Tomita, and Y. Motome, Phys. Rev. B **90**, 165119 (2014).

[43] W. A. Harrison, *Electronic Structure and the Properties of Solids* (Dover, New York, 1989).
[44] G. Khaliullin, P. Horsch, and A. M. Oleś, Phys. Rev. Lett. **86**, 3879 (2001).
[45] P. Horsch, G. Khaliullin, and A. M. Oleś, Phys. Rev. Lett. **91**, 257203 (2003).
[46] G. Khaliullin, Prog. Theor. Phys. Suppl. **160**, 155 (2005).
[47] J. C. Slater and G. F. Koster, Phys. Rev. **94**, 1498 (1954).
[48] The mechanism by which a 3-1 ground state appears is different from previous work, where a partially ordered monopole crystal has been proposed [49–51] and multiferroic behavior discussed [52].
[49] M. E. Brooks-Bartlett, S. T. Banks, L. D. C. Jaubert, A. Harman-Clarke, and P. C. W. Holdsworth, Phys. Rev. X **4**, 011007 (2014).
[50] L. D. C. Jaubert, SPIN **05**, 1540005 (2015).
[51] L. D. C. Jaubert and R. Moessner, Phys. Rev. B **91**, 214422 (2015).
[52] D. I. Khomskii, Nat. Commun. **3**, 904 (2012).
[53] C. L. Henley, Annu. Rev. Condens. Matter Phys. **1**, 179 (2010).
[54] C. Castelnovo, R. Moessner, and S. Sondhi, Annu. Rev. Condens. Matter Phys. **3**, 35 (2012).